Multi Array, Conformable Ultrasound Patch for Soft Tissue Imaging

by

David Mejorado III

SB, Electrical Science and Engineering, Massachusetts Institute of Technology, 2020

Submitted to the Department of Electrical Engineering and Computer Science
in partial fulfillment of the requirements for the degree of

Master of Engineering in Electrical Engineering and Computer Science

at the

MASSACHUSETTS INSTITUTE OF TECHNOLOGY

June 2021

Author .....
Department of Electrical Engineering and Computer Science
May 20, 2021

Certified by .....
Canan Dagdeviren
Assistant Professor, MIT Media Lab, LG Career Development Professor of Media Arts and Sciences
Thesis Supervisor

Accepted by .....
Katrina LaCurts
Chair, Master of Engineering Thesis Committee

Multi Array, Conformable Ultrasound Patch for Soft Tissue Imaging

by

David Mejorado III

Submitted to the Department of Electrical Engineering and Computer Science
on May 20, 2021, in partial fulfillment of the
requirements for the degree of
Master of Engineering in Electrical Engineering and Computer Science

Abstract

Medical ultrasound imaging is a rapidly growing field due to its safety and affordability when compared to other imaging modalities such as MRI and X-Ray. Ultrasound transducers are made in various configurations from dense 2-D arrays for volumetric imaging to single element needle like transducers for intravascular imaging. The performance of an ultrasound transducer is dictated by the properties of the piezoelectric material being used. One current drawback to ultrasound is that it is heavily operator dependent. This has motivated research into developing ultrasound systems that are conformable to the body and capable of obtaining relevant information without the need for an operator. This thesis explores the design and fabrication of a locally rigid globally flexible ultrasound patch using novel piezoelectric ceramics. The ceramics are fabricated into 64 element linear arrays transducers and then their electrical impedance and acoustic properties are characterized. Individual and groups of transducers are then used to image a flat and a curved ultrasound imaging phantoms via the Verasonics system.

Thesis Supervisor: Canan Dagdeviren
Title: Assistant Professor, MIT Media Lab, LG Career Development Professor of Media Arts and Sciences

Acknowledgments

There are many people who have supported me and that I would like to extend my gratitude. First, I am extremely grateful to my PI and thesis advisor Canan Dagdeviren for her constant support and encouragement. Without her guidance none of this would have been possible. I would also like to thank everyone in my research group at the Media Lab Conformable Decoders for their friendship and intellectual guidance. Additionally, I would like to specifically thank Lin Zhang for his mentorship. Next, I would like to thank our collaborators in CURT at MGH who were Viksit Kumar, Scott Schoen, and Alex Benjamin; without them many experimental results would not have been possible to obtain.

In addition I would like to thank my mom, dad, and sisters for their love and encouragement in my pursuit of a graduate degree. A big thank you to my girlfriend Jesse for supporting me through the long work hours and reminding me to take breaks. And finally, thank you to all my friends at MIT who I shared this experience with.

Contents

List of Figures

List of Tables

Chapter 1

Introduction

Medical diagnostics and research have been greatly aided by technology that enables non-intrusive visualization of the body's internal structures. Medical imaging can be achieved through different approaches ranging from magnetic resonance imaging (MRI) to x-ray imaging, to ultrasonic imaging. Ultrasound technology is incredibly versatile and widely used in developing diagnosis as well as various therapeutic applications. Unlike computed tomography and x-ray imaging, however, ultrasound has no risk of radiation exposure, and it is both less costly and time consuming than an MRI [17, 13]. Additionally, ultrasound imaging allows for real-time imaging and holds high potential for compact and portable imaging systems. Ultrasonic waves can be generated through a variety of physical phenomena, nevertheless the piezoelectric effect is the most commonly used to actuate and sense ultrasonic signals. At the core of medical ultrasonic technology is the ultrasound transducer. The structure and design of ultrasound transducers can vary from single element transducers to dense two-dimensional arrays with thousands of elements and with a wide range of ultrasonic frequencies [17]. Ultrasound's wide variety of applications results in a variety of ultrasound transducer designs that optimize to meet the specific requirements of each use case.

1.1 Piezoelectricity

The piezoelectric effect is a linear relationship where the mechanical strain (S) and stress (T) of a material are coupled to the electric field (E) and electric displacement (or electric charge density D) [26]. The piezoelectric effect is a reversible process which exhibits two effect: direct piezoelectric effect (the internal generation of electrical charge is generated from an applied mechanical stimulus), and converse piezoelectric effect (the internal generation of a mechanical strain is generated from an applied electrical field), expressed by Equation 1.1 [21].

$$\begin{bmatrix} Converse \\ Direct \end{bmatrix} = \begin{bmatrix} S \\ D \end{bmatrix} = \begin{bmatrix} s^E & d \\ d & \epsilon^T \end{bmatrix} \begin{bmatrix} T \\ E \end{bmatrix} \tag{1.1}$$

where s^E is the compliance under a constant electrical field, ϵ^T is the dielectric permittivity under a constant stress, and d is the matrices for direct and converse piezoelectric coefficient. The piezoelectric coefficient for each materials has its own value with respect to its crystal orientation.

1.2 Material Parameters for Ultrasound Transducers

There are several parameters used to evaluate the performance of piezoelectric material. For imaging transducers, the key material parameter is the electromechanical coupling factor, which is closely related to device bandwidth and sensitivity. In addition, the dielectric permittivity is a critical parameter in order to match the electrical impedance of transducer to that of driving electronics. Temperature and field stabilities are also important for ultrasound transducers, since the dielectric permittivity changes as a function of temperature and field, resulting in the variation of electrical impedance of device.

While there is an abundance of parameters used in material science to describe the piezoelectric properties the following are the most relevant for describing ultrasonic

transducers: C_{s33}, is the clamped capacitance; ϵ_{s33}, the clamped dielectric permittivity; A, the area; t, the thickness; k_t, the thickness-mode electromechanical coupling coefficient; e_{33}, the piezoelectric stress constant; c_{D33}, the elastic constant; ω_0, the resonant frequency; c_p, the speed of sound inside the piezoelectric material; Z_a, the acoustic impedance; and ρ, the density.

As the piezoelectric material itself can be considered as a capacitor, the corresponding ultrasonic transducer is a capacitor structure. The clamped capacitance of an ultrasonic transducer is determined by the clamped dielectric permittivity, the area and thickness of the piezoelectric material. To maximize the power transmission, the input electrical impedance of the ultrasonic transducer at the designated frequency should be real and its input resistance should match the electrical impedance of the source (normally 50 Ω in termination).

The electromechanical coupling coefficient k is an indicator of the effectiveness with which a piezoelectric material converts electrical energy into mechanical energy and vice versa. It is not a constant material parameter, but instead of depending upon the shape of the material. For example, the k coefficient of a material in a rod form is higher than that in a plate form [19]. In transducer design, a high k value is desirable for better energy conversion and improved bandwidth. The resonant frequency and the acoustic impedance of a material are determined by the speed of sound inside itself which is an inherent property of the material. It is mentioned above that the impedance matching between the transducer and the propagating medium is very important to improve the transducer performance.

Besides selecting the appropriate piezoelectric material for a designated transducer, the configuration of the transducer element can also be tailored to approach the desired transducer performance. Piezoelectric 1-3 [12, 3]and 2-2 [9] composites are also commonly used in transducer technology. The higher k coefficients and better impedance matching can lead to higher transducer sensitivity and improved bandwidth.

1.3 Conformable Ultrasound Imaging Devices

Biomedical imaging has a wide range of applications ranging from patient care such as detection and diagnosis of foreign bodies and fractures to studies of biological structure and function to address fundamental questions in biomedicine [10]. Because of its improved image resolution, high frequency ultrasonic imaging has been used as a clinical tool for examination of the skin, the anterior segment of the eye, vascular system, etc [18]. Despite the numerous benefits, conventional ultrasound technology still suffers from drawbacks such as high operator dependence, the accompanying measurement variability and inability to cover curved human body parts or perform whole-organ imaging with high spatiotemporal resolution due to probe rigidity [15]. As a result, there is a need to develop flexible and conformable ultrasound transducer arrays that are operator-independent and provide seamless contact to the curvilinear surfaces on the human body.

A conformable ultrasound imaging devices necessitates a complex integrated system consisting of: flexible/stretchable substrates, conducting electrodes, transducers, and encapsulation materials. For implementing general flexible electronics, (1) elastic materials and (2) stretchable/flexible structure are the two approaches to achieve mechanical flexibility and stretchability. However, there are many limitations and requirements to make ultrasound transducers flexible, even stretchable.

Traditional ultrasound transducers are all based on rigid substrates, while two-dimensional arrays do not conform to the human body shape and line-arrays are difficult to operate. The existing flexible devices have some defects in both tensile and ultrasonic properties, and the process is relatively complex. To make the ultrasound patches flexible and stretchable, available methods are similar to other comfortable electronics. Two approaches on material science and electronic engineering have been employed: (1) flexible piezoelectric materials and (2) rigid piezoelectric elements on stretchable/flexible structures. Specifically, to realize large volume and operator-independent acquisition, conformable ultrasound device should meet mainly three requirements: (1) physical and electronic requirements: the array must be flexible or

stretchable enough to seamlessly physical adhere and reliably acoustic contact over its entire surface area; (2) beam generating and sound field: location of the transducer element positions and orientations; and (3) data integrity and signal processing: image acquisition must be of high quality to allow post-scan clinical assessment without regard for scanning geometry.

1.4 Prior Work

As previously mentioned the two approaches to make ultrasound devices flexible and stretchable is : (1) using flexible piezoelectric materials such as PVDF and (2) embedding rigid piezoelectric elements in stretchable/flexible materials such as PDMS and polyimide.

Flexible Piezoelectric Materials

Among the flexible piezoelectric ultrasound transducer systems, most are composed with PVDF. Compared to conventional bulk piezoelectric ceramics such as PZT, PVDF and its copolymer offer advantages such as high mechanical flexibility, broad bandwidth and low acoustic impedance. Flexible linear and two dimensional transducer arrays made of PVDF and its copolymer have been used to perform imaging of a wide variety of human tissues such as the breast [11, 5], femoral artery [6], eyes [16, 7, 19] and cartilage [12].

Rigid Transducer Stretchable/Flexible Substrate

Conventional piezoelectric materials such as PZT exhibit excellent electromechanical performance and are well-studied, but they suffer from high modulus that makes them ill-suited for integration with curvilinear biological surfaces. As fabrication techniques and processing technologies advance, bulky piezoelectric materials are able to be manufactured in smaller dimensions which enables the integration of bulk ceramic materials in flexible or stretchable substrates. However, even when rigid piezoelectric elements are embedded in stretchable or flexible materials, the overall system is of-

ten only flexible but not conformable and can often present mechanical detachment issues. Dann et al. fabricated a flexible 2D ring annular array which consisted of PZT elements mounted on silicon islands held together with polyimide joints and encapsulated in a thin layer of parylene-C film[8]. The polyimide/parylene joints were capable of withstanding more than 10,000 cycles of iteratively flexing about an angle of 60^{o} without deterioration. The flexible ring annular array provides enhanced focusing capabilities by being able to perform both electronic and mechanical beam steering/focusing and is aimed for applications such as fracture detection in extremities and evaluation of shrapnel and wound tracts.

Utilizing similar device structure with polyimide joints, Bennett et al. fabricated a linear transducer array that can be curved around an index finger and withstand 1,000 bending cycles around a cylinder of 1 cm in diameter while Singh et al. evaluated a PZT transducer array mounted on copper-cladded polyimide flexible printed circuit substrate[2, 18]. However, even though the spaced island design allowed the device to be bent and curved, the polyimide flexible joints were not robust enough and could not be stretched.

1.5 Overview

This research aims to develop a multi-transducer conformable ultrasound imaging system utilizing novel piezoelectric ceramics. Preliminary studies on this ceramic have shown promising results indicating to an improvement in performance when compared to other PZT ceramics. Rigid ultrasound transducers were fabricated from these novel ceramics. The goal is then to embed these locally rigid transducers into a globally flexible substrate. Chapter 2 details the ultrasound transducer design, and reports the electrical and acoustic characterization of eight 64 element transducers. In chapter 3, the transducers are interfaced with a commercial ultrasound imaging system in order to image an ultrasound characterization phantom. Chapter 4 describes the methods for designing and fabricating a five transducer patch, and asses the image acquisition of this design on a curved ultrasound imaging phantom. Fi-

nally, Chapter 5 summarizes all of the results and describes remaining challenges and possible solutions.

Chapter 2

Fabrication and Characterization

This chapter will briefly discuss the design and fabrication process of the ultrasound transducer from bulk piezoelectric material. Then it will describe in depth the characterization procedures and results of eight transducers that were fabricated.

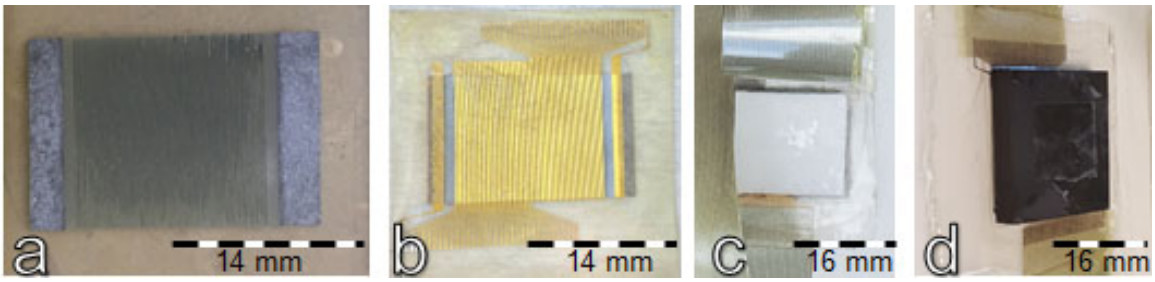

Figure 2-1: (a) top view after dicing (b) top view after electrode deposition (c) top view with matching layer (d) bottom view of transducer with backing layer

2.1 Device Design and Fabrication

The design of these transducers can be separated into two parts. The first describes the dimensions of the array which can be found in Table 2.1. With these design parameters the bulk piezoelectric material is polished to reach a desired thickness and diced to create the individual elements. Additionally, Au/Cr electrodes are deposited over the individual elements via electron beam vapor deposition using a photoresist mask. Figure 2-1(a) show the transducer prior to electrode deposition and (b) after

electrode deposition.

The second part of the design and fabrication is ensuring that ultrasound waves can properly propagate into human tissue. This is accomplished by adding matching layers to the transducer that match the acoustic impedance of the piezoelectric material to that of the skin. Additionally, a backing layer is also added to ensure ultrasonic energy is only being propagated forward. This is accomplished by selecting a backing layer that rapidly attenuates the ultrasound waves that propagate through it. The details to these layers is listed in Table 2.2. Figure 2-1(c,d) show the transducer with its matching and backing layer respectively.

Table 2.1: Overview of the parameters used in the transducer's array design

Parameters	Value	Explanation
Working frequency (*f*)	3.5 MHz	Compare with C5-2 used in the bladder imaging
Wavelength (λ)	440 μm	$\lambda = c/f$ 1540/3.5 = 440 μm
Pitch	220 μm	Meet the requirement of $\lambda/2$ for phased array
Element width (*w*)	170 μm	Determinted by the thickness and vibration of the blade
Kerf	50 μm	Determinted by the thickness and vibration of the blade
Length (*l*)	14 mm	220 μm × 64 = 14.08 mm
Thickness (*t*)	560 μm	Frequency constant = thickness × working frequency
G = *t*/*w*	3.23	Meet the requirement of *t*/*w* > 3 for better thickness vibration
Height (*h*)	15 mm	1) $N = H^2/4\lambda$: The required focal depth >10 cm. H > 13.2 mm 2) Impedance match. The impedance at resonance frequency is around 50 Ω

Finally, in order to make the gold electrodes accessible for characterization an Anisotropic conductive film (ACF) is used to electrically connect the transducers to a 2-layer PCB as seen in Figure 2-2. The ACF connection is done by aligning the individual traces on the film to the electrodes on the transducer and then heat bonding. After this step the transducer is ready to begin characterization.

Table 2.2: Summary of material properties used in the transducer

Function	Materials	Thickness (mm)	Sound velocity (m/s)	Density (kg/m^3)	Acoustic impedance (MRayls)
1st matching layer	Epoxy 301/ZrO_2 powder	0.24	2780	2890	8.22
2nd matching layer	Epoxy 301	0.22	2602	1150	2.98
Backing layer	Esolder 3022	1.5	1890	3160	5.98
Load medium	Water	-	1540	1000	1.50

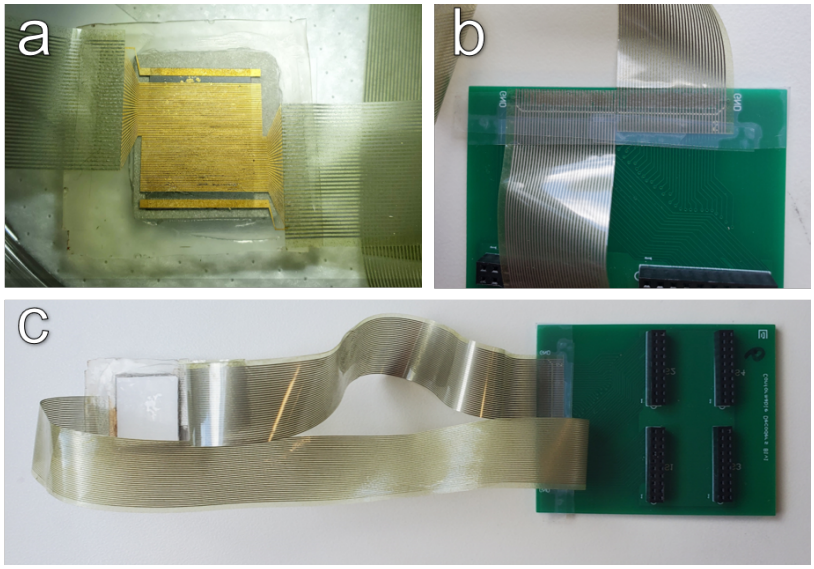

Figure 2-2: (a) Close up of a transducer's top surface after electrode deposition and after ACF bonding (b) ACF bonded to board 1 (c) Image of fully fabricated transducer

For each characterization modality the results can be summarized at three different levels, individual elements, entire transducers, and across all the fabricated transducers. For each of the different measurements representative data sets will be presented in detail and the broader results will be summarized.

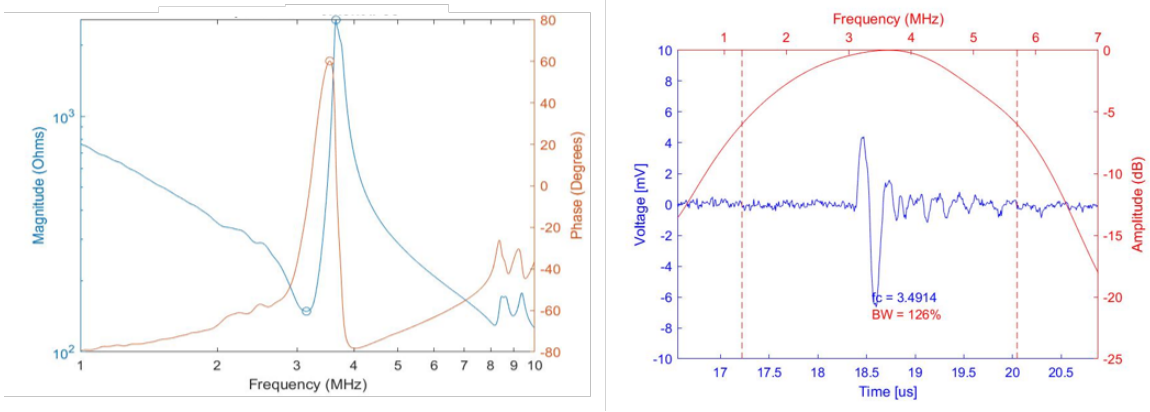

Figure 2-3: Single Element Characterization for element 7 of transducer #5

2.2 Impedance Analysis

Electrical impedance of the fabricated linear array was measured in air using an impedance analyzer (Agilent E4991A, Agilent Technologies). Each transducer's individual element is measured individually resulting in 64 waveforms that describe the entire array. This measurement can be made as soon as the gold electrode deposition is completed, however the resulting measurement varies as the additional fabrication steps are completed. Prior to each measurement the impedance analyzer is calibrated and each element is scanned over a frequency range of 1MHz-6MHz.

The impedance of each element is represented by a phase and magnitude as seen in Figure 2-3(left). From this two key parameters can be obtained the elements resonance and anti-resonance. Due to this being an impedance plot a negative peak indicates a resonance where as a positive one indicates the anti-resonance. In Figure 2-3 the resonance is at $f_R = 3.43$ MHz with an impedance magnitude of 319Ω while the anti-resonance is at $f_A = 4.16$ MHz with 880Ω. From these values the k_{eff} parameter for piezoelectric devices can be estimated using equation 2.1[20].

$$k_{eff} = \sqrt{1 - \frac{f_R^2}{f_A^2}} \tag{2.1}$$

In this case $K_{eff} = 0.57$. Furthermore this calculation is made for every element in a transducer. The results of this are presented in Figure 2-4. Figure 2-4(a-b) plots the impedance magnitude of each individual element in 3D space with the new dimension being element #. This shows how the waveform varies across the transducers, and makes trends easier to notice. In this case the impedance at the anti-resonance seems to be decrease and then increase. The continuity in the changes indicates that this might be caused by an unevenness in the surface or thickness of the piezoelectric ceramic. Additionally, the empty spaces indicate a lack of proper electrical connection between Board 1 and the individual element. This might be caused by the degradation of the ACF cable or an deformity in the gold electrode. For each transducer a yield for successful connections can then be described. Finally, Figure 2-4(c-e) plots the resulting resonance, anti-resonance, and k_{eff} values. A

Table 2.3: Summary of impedance characterization across 8 transducers

Array Num		Resonance			Anti-Resonance			K	Yield [%]
		Freq [MHz]	|Z|	Phase [°]	Freq [MHz]	|Z|	Phase [°]		
1	Avg	3.45	360	-48	4.22	756	-51	0.57	84
	Std	0.08	202	8	0.14	336	7	0.03	
2	Avg	3.40	310	-47	3.98	636	-49	0.52	94
	Std	0.11	77	7	0.08	63	8	0.02	
3	Avg	3.31	251	-39	4.17	464	-40	0.61	84
	Std	0.14	35	4	0.11	101	6	0.03	
4	Avg	3.42	136	-12	4.05	2,772	-6	0.54	84
	Std	0.07	8	3	0.07	207	6	0.01	
5	Avg	3.44	195	-21	4.23	990	-23	0.58	92
	Std	0.05	28	4	0.03	169	5	0.01	
6	Avg	2.88	213	-27	3.61	715	-32	0.60	71
	Std	0.14	53	8	0.31	289	9	0.04	
7	Avg	3.29	234	-30	3.93	724	-37	0.54	93
	Std	0.10	24	3	0.17	95	7	0.03	
8	Avg	3.15	146	-11	3.68	2,829	5	0.51	98
	Std	0.06	30	5	0.07	335	10	0.02	

summary of all of these parameters can be found in Table 2.3. From this table it is clear that there are inconsistencies across the transducers resonance and anti-resonance frequency, which is due to a non-uniform thickness. Despite this the k_{eff} does not vary as much. It is also important to note that no transducer reached a 100% yield on the electrical connection.

2.3 Acoustic Performance

The test setup for this measurement is described in Figure 2-5. The acoustic pressure generated by the phased array was measured inside a 10-gallon water tank filled with degassed water. The transducer was fixed to the side of the tank using double-sided tape and was driven by the Verasonics Vantage Research Ultrasound System. A hydrophone (Onda HGL-0200 Capsule Hydrophone) was used to measure the acoustic pressure. The hydrophone's generated voltage is fed through a preamplifier (Onda AG-2010 Hyrdrophone Preamplifier) which is then read and captured using an oscilloscope (Tektronix 3 Series MDO32). Finally, a trigger signal was also output from

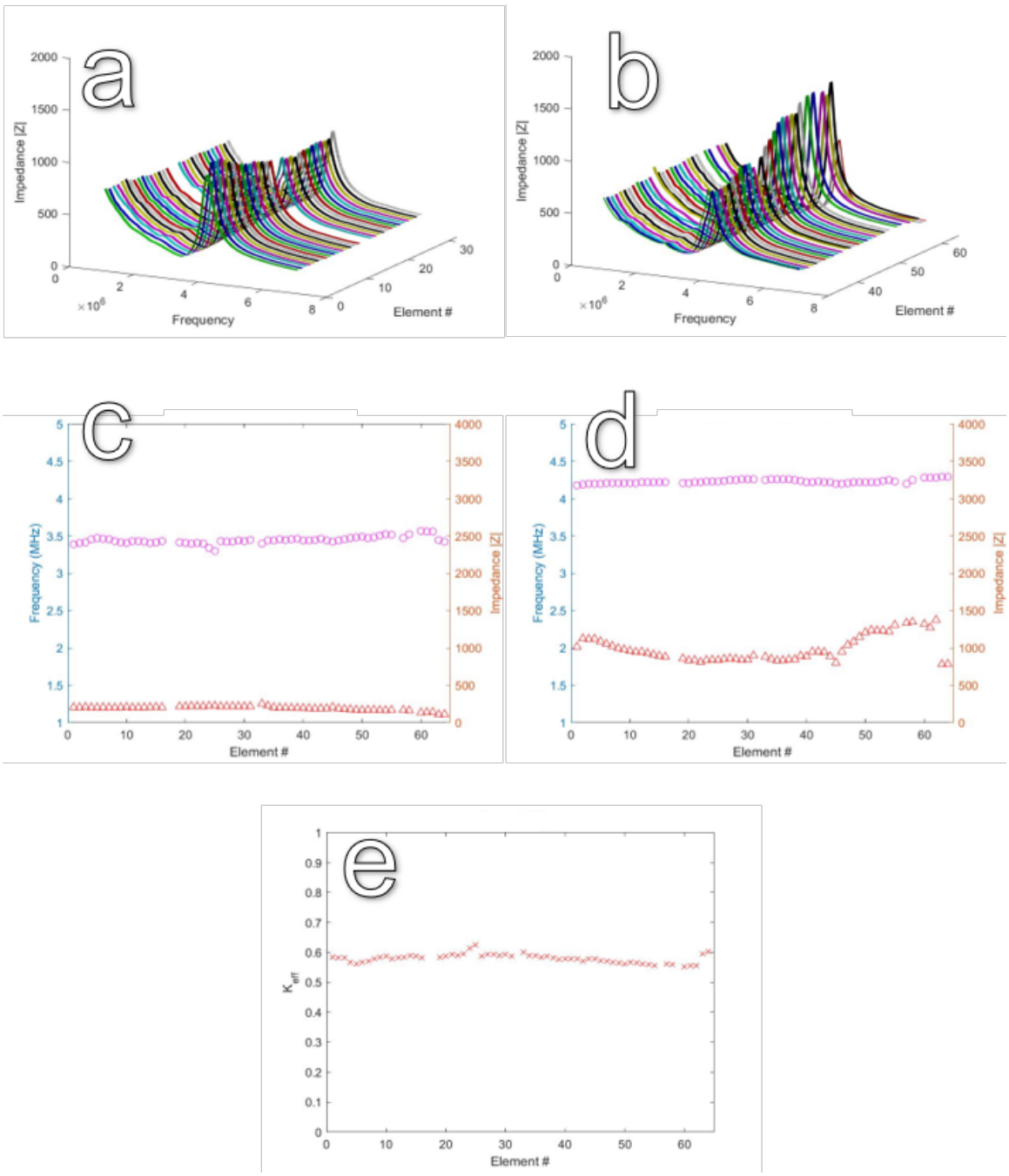

Figure 2-4: Summary of electrical impedance characterization of transducer #5 (a-b) Impedance Magnitude (c) Resonance (d) Anti-resonance (e) K_{eff}

Verasonics into the oscilloscope to facilitate data capture.

A test setup made up of optical components was built as a custom holder for the hydrophone. The holder is mounted on a 3-axis motion stage which is fixed to an optical breadboard for support. The motion stage provided a resolution of 0.5 mm

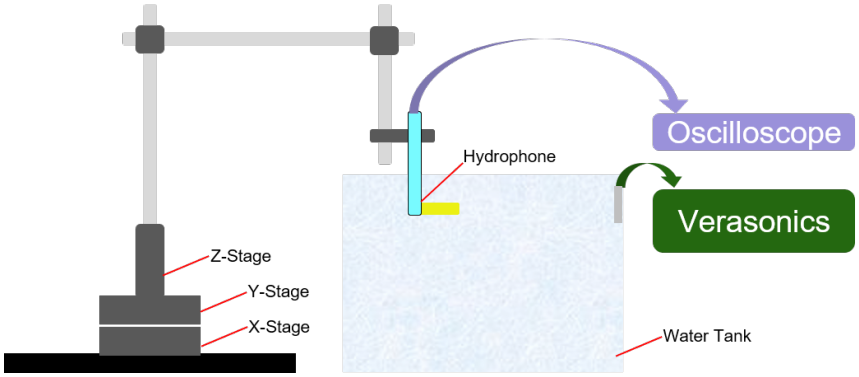

Figure 2-5: Diagram describing the 3-axis motion stage used to measure acoustic pressure generated by an ultrasonic transducer inside a water tank

translation per revolution in the x-y axis over 25 mm and 0.635 mm translation per revolution on the z axis over 16.4 mm. The fully built test bed is shown in Figure 2-6.

First the transducer was connected to Verasonics and fixed inside the water tank. The hydrophone was then immersed in the water and positioned 5cm away from the transducer. Next, the transducer was driven with a single cycle 3.5 MHz pulse, and delays were introduced across the transducers in order to focus the transmit beam. Measurements were then taken with the transmit beam focused at 3cm, 4cm, 5cm, 6cm, and 7cm. This was repeated two more times such that for $X_h = HydrophonePosition$ 5 measurements were taken with transmit beam focused at

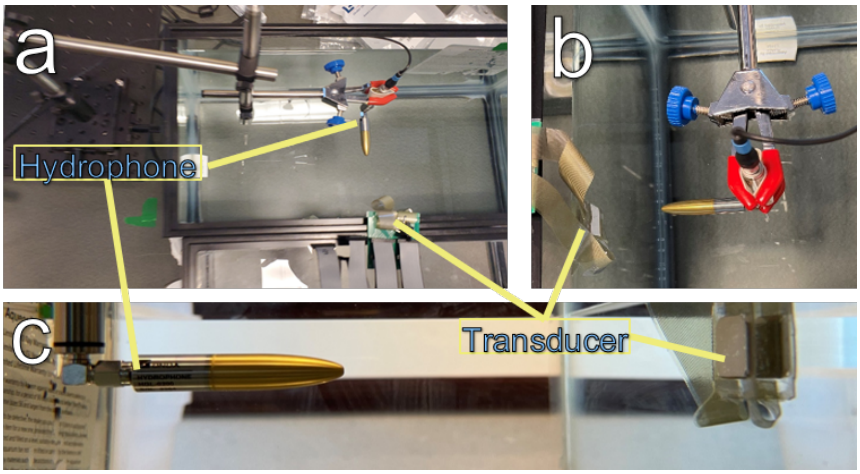

Figure 2-6: Images of experimental test setup used to perform acoustic pressure measurement(a) top view (b) right side view (c) left side view

Table 2.4: Summary of acoustic pressure data collection scheme

Hydrophone Position	Transmit Beam Focal Point				
5 cm	3 cm	4 cm	5 cm	6 cm	7 cm
7 cm	5 cm	6 cm	7 cm	8 cm	9 cm
10 cm	8 cm	9 cm	10 cm	11 cm	12 cm

$X_h + \delta_x$ for $\delta_x = [-2, -1, 0, 1, 2]$. Table 2.4 summarizes all the positions and respective focal points that are measured.

The raw data from the hydrophone is processed to convert the voltage into acoustic pressure using sensitivity values provided by the manufacturer. First the voltage is derated by taking into account the attenuation of the medium. Figure 2-7 shows this voltage waveform recorded at three different position. From this waveform peak rarefactional pressure, p_r, is calculated and used to obtain three characteristic parameters: Mechanical Index (MI), Spatial peak temporal average intensity (I_{SPTA}), and Spatial peak pulse average intensity (I_{SPPA}) [14, 4, 1]. These parameters are used by regulation agencies like the FDA to ensure that ultrasound transducers are not delivering harmful levels of ultrasonic energy into the body. Calculations for these parameters include details like pulse duration (PD) and pulse repetition frequency

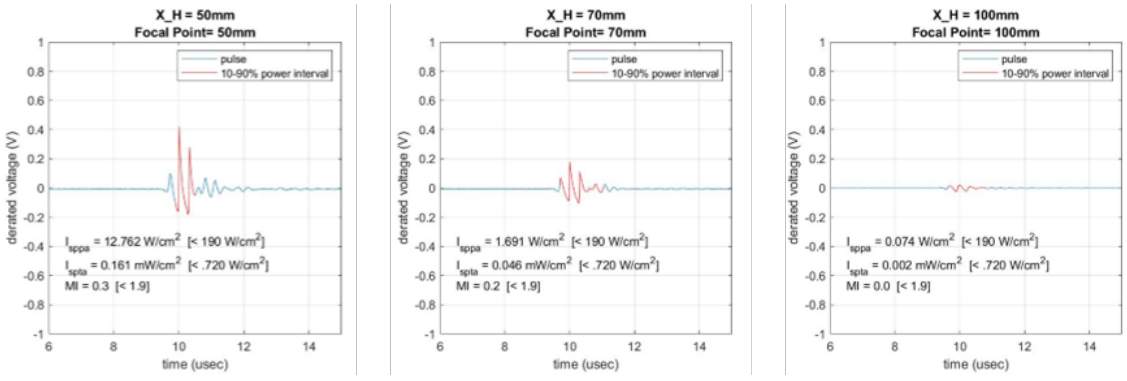

Figure 2-7: Acoustic pressure data for a single transducer at 3 points

(PRF) and are carried out as follows :

$$PD = 1.25 \times (t_{90} - t_{10}) \qquad PRF = 16Hz \qquad f_c = 3.5MHz \tag{2.2}$$

$$I_{SPPA} = \frac{PII_d}{PD} \qquad I_{SPTA} = PII_d \times PRF \qquad MI = \frac{p_r}{\sqrt{f_c}} \tag{2.3}$$

where PII_d is the pulse integral intensity or the pulse power, while t_{10} and t_{90} are the times when the amplitude is bellow 10% and 90% below peak PII_d respectively. A summary of these parameters across all transducers is shown in Table 2.5 and in Figure 2-8. From these it is clear that the custom transducers pose minimal risk to the body given how for each parameters the results are distributed well below the recommended safety limits[1].

Table 2.5: Summary of Acoustic measurements across 8 transducers

Array Number	ISPTA (mW/cm2)			ISPPA (W/cm2)			MI (unitless)		
	Max	Mean	St. Dev.	Max	Mean	St. Dev.	Max	Mean	St. Dev.
1	0.064	0.049	0.011	6.862	5.322	1.37	0.214	0.189	0.022
2	0.120	0.044	0.037	12.107	4.439	3.850	0.295	0.185	0.079
3	0.057	0.021	0.018	8.233	2.568	2.673	0.216	0.119	0.058
4	0.079	0.020	0.024	8.776	2.204	2.736	0.196	0.102	0.052
5	0.072	0.026	0.019	10.096	3.295	2.812	0.266	0.150	0.068
6	0.057	0.027	0.02	5.932	2.296	2.004	0.150	0.127	0.057
7	0.164	0.053	0.054	13.232	2.772	3.924	0.330	**0.162**	**0.100**
8	0.082	0.027	0.027	9.626	2.896	3.227	0.255	0.123	0.080
Suggested FDA level	0.72			190			1.9		

2.4 Pulse/Echo

A pulser/receiver (JSR Ultrasonics DPR 300) was used to individually excite single elements from a transducer with an electrical impulse of $9J$, a reputation rate of 100 Hz and 182 Ω damping factor, and the previously described hydrophone and pre-amplifier was used as the receiver. The hydrophone output was measured and recorded on an oscilloscope (PicoScope 5000 series). A modified experimental setup was used to take this measurement as shown in Figure 2-9 and Figure 2-10. The

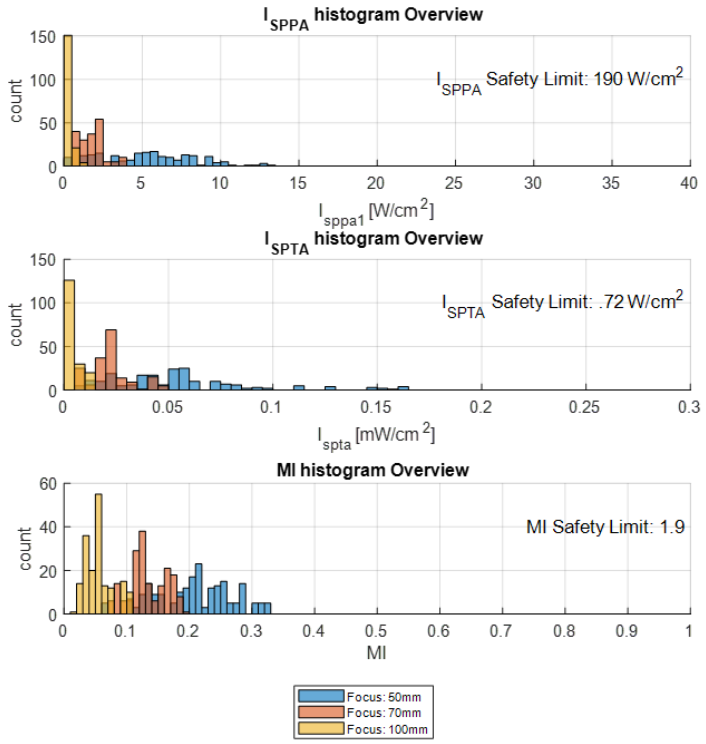

Figure 2-8: Three histograms describing the distribution of acoustic energy at multiple distances and focal points over all 8 transducers

transducer was fixed to the bottom of a glass container filled with degassed water and the hydrophone was suspended above the transducer at a fixed distance.

At the start of each data acquisition the hydrophone was aligned over the transducer by moving the 2-axis stage that the hydrophone is mounted on and maximizing the amplitude of the hydrophone output. For each transducer measured random 4 independent elements were selected across the transducer to represent the transducer. The data stored data was then processed in Matlab to calculate its frequency spectra. From this, upper f_u and lowerf_u -6 dB frequency bands were identified as well as the center frequency:

$$f_c = \frac{f_u + f_l}{2} \tag{2.4}$$

$$BW = \frac{f_u - f_l}{f_c} \times 100 \tag{2.5}$$

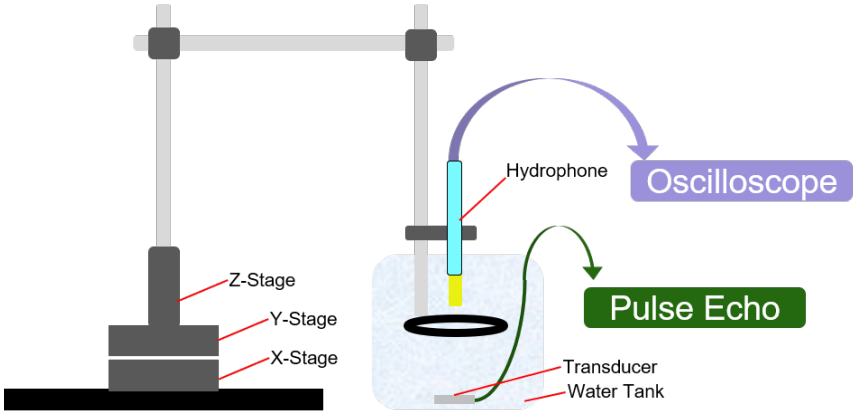

Figure 2-9: Diagram of test-bed for pulse/echo measurement of individual transducer elements

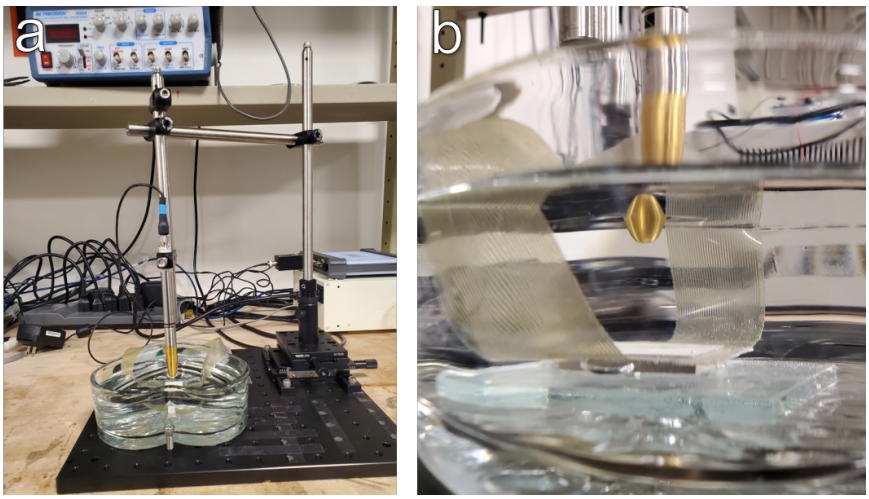

Figure 2-10: Pictures of test-bed for pulse/echo measurement of individual transducer elements(a) front view (b) close up side view

Given the parameters previously discussed in Table 2.1 the goal for each transducer was to achieve a working frequency of 3.5 MHz. In Figure 2-11 the pulse echo results of transducer 4 are shown. For these 4 elements there is minimal variation and they all include 3.5 MHz in their bandwidth. However, this was not the case across all transducers. Table 2.6 details the center frequency and bandwidth across all transducers. From this it is evident that most transducer met the criteria of including 3.5 MHz in their bandwidth even if the center frequency was not consistently 3.5 MHz. Additionally, some transducers are showing a large standard deviation within the 4 elements.

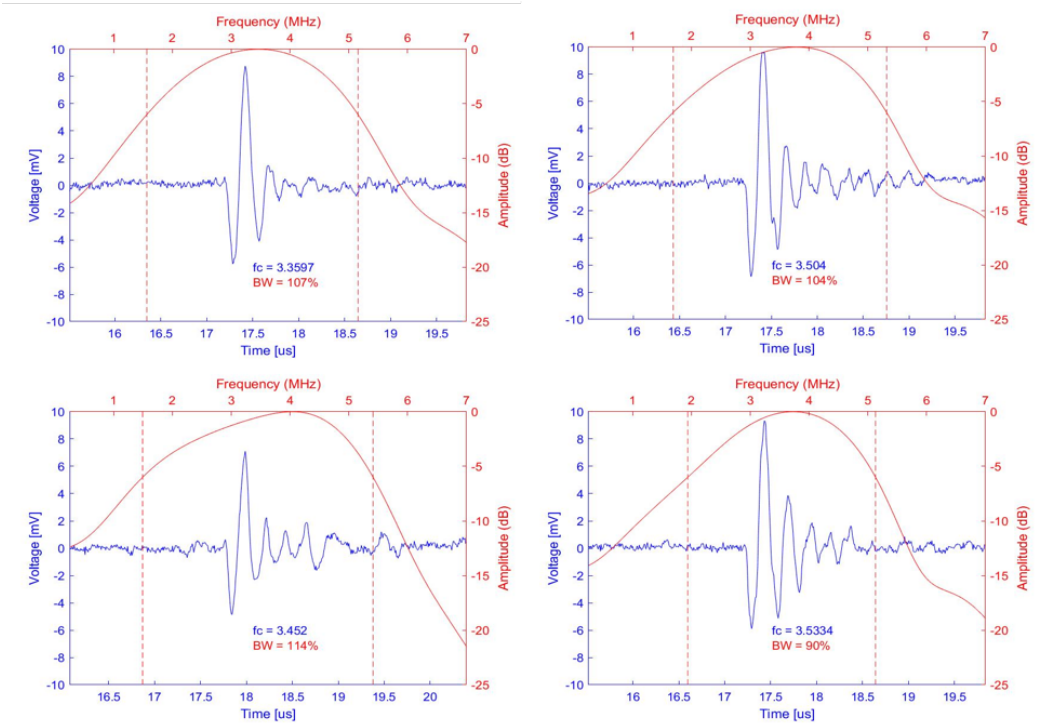

Figure 2-11: Pulse echo data from 4 elements in a single transducer # 4

Table 2.6: Summary of pulse/echo characterization across 8 transducers

Array Num		Element 1	Element 2	Element 3	Element 4	Average	Std.
1	Fc [MHz]	2.76	3.56	3.5	3.95	3.44	0.50
	Bandwidth	200%	98%	101%	79%	120%	55%
2	Fc [MHz]	3.12	3.18	3.00	3.14	3.11	0.08
	Bandwidth	104%	108%	114%	89%	104%	11%
3	Fc [MHz]	4.21	3.46	3.65	3.64	3.74	0.33
	Bandwidth	62%	111%	101%	83%	89%	22%
4	Fc [MHz]	3.45	3.53	3.50	3.36	3.46	0.07
	Bandwidth	114%	90%	104%	107%	104%	10%
5	Fc [MHz]	3.37	3.00	3.13	3.29	3.20	0.17
	Bandwidth	135%	141%	108%	116%	125%	16%
6	Fc [MHz]	2.80	2.57	2.61	2.74	2.68	0.11
	Bandwidth	101%	114%	114%	112%	110%	6%
7	Fc [MHz]	3.05	3.35	3.13	3.26	3.20	0.13
	Bandwidth	94%	93%	92%	93%	93%	1%
8	Fc [MHz]	3.30	3.49	3.36	3.36	3.38	0.08
	Bandwidth	105%	126%	98%	113%	111%	12%

Chapter 3

Ultrasound Imaging on Flat Surface

All of the image acquisition was carried out using a Verasonics Vantage Ultrasound Research System at the Center for Ultrasound Research and Translation (CURT) at MGH. Collaborators at this center facilitated the use of this system during the data acquisition process. The Verasonics system is capable of driving two transducers with up to 128 elements each. Additionally, various beamforming techniques can be implemented for real time imaging and raw data acquisition. The entire system is programmed in Matlab through scripts and a Graphic User Interfaces. This chapter follows the design and construction of a connector to interface the lab made transducers with the commercial system, and an assessment of the images obtained on a flat ultrasound phantom.

3.1 Single Transducer UTA Connection

Ultrasounds transducer interface with Verasonics via a Universal Transducer Adapter (UTA). In order to interface the fabricated transducers with Verasonics, an adaptable connector was designed and built that was UTA compatible. Figure 3-1 describes the overall design and signal path from Verasoncics to a transducer. This design allows for the transducer in use to be interchangeable. An additional aspect to note is the ordering of the elements in the UTA connector. The inherit ordering of a UTA connector is not sequential and therefore does not follow the physical structure of a

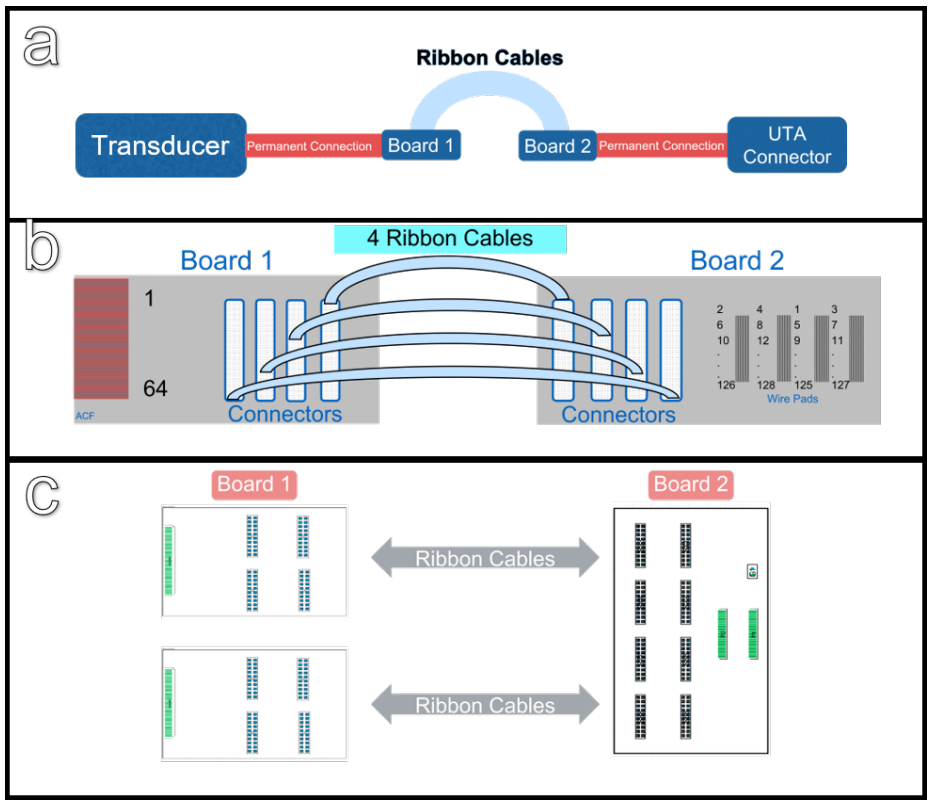

Figure 3-1: (a) High level diagram describing the signal path (b) detailed diagram with separated signal paths (c) Schematic of PCB boards used

transducer. To solve this Board 2, a 4 layer printed circuit board (PCB), takes a sequential ordering at its inputs and reroutes the signals to match what the UTA connector expects.

A commercial ultrasound transducer with a UTA connection was deconstructed and modified to meet this need. The connector is capable of supporting up to 128 individual elements. The final design grouped these signals into 8 groups of 16. Each individual signal line was removed off of the original printed circuit board (PCB) and soldered onto PCB 2. Figure 3-2 shows the deconstruction of the commercial probe and construction of the previously described connector. This PCB interfaces via ribbon cables to the transducer's complementary PCB. Due to each transducer consisting of 64 elements two transducers could be connected in parallel with this interface

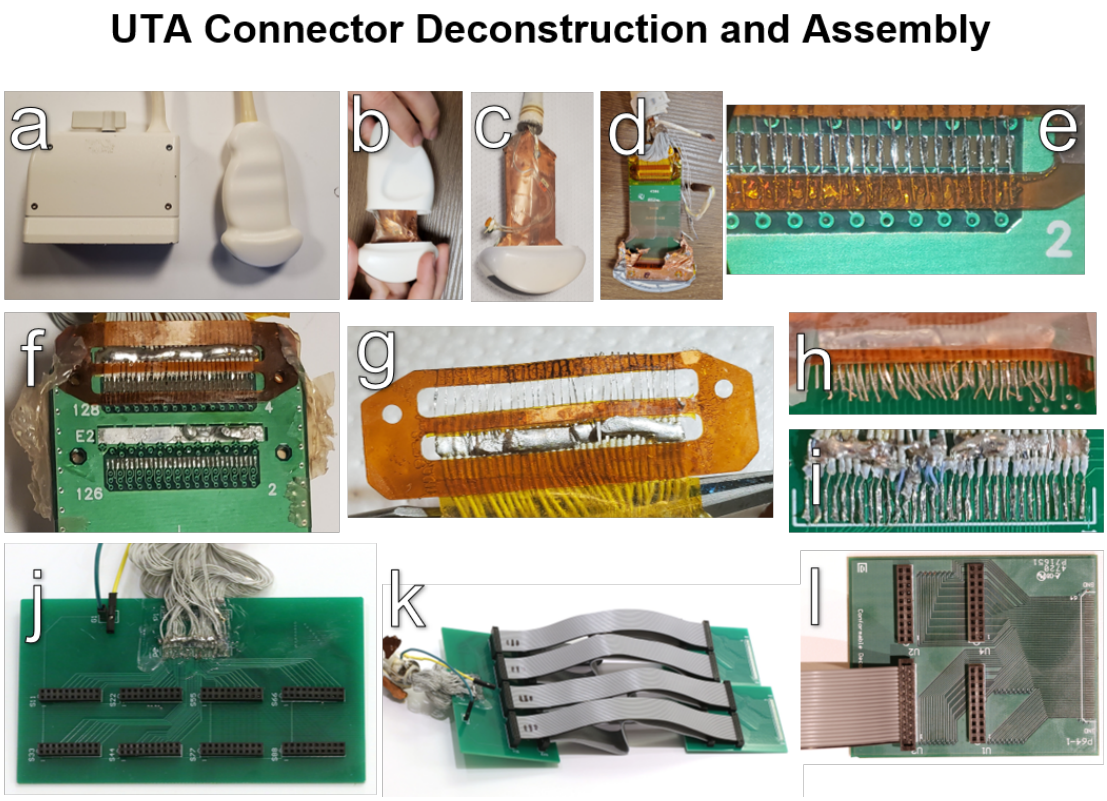

Figure 3-2: (a-g) Disassembly of a comercial ultrasound probe with a UTA connection. (h-i) Removal of wires from comercial PCB onto custom PCB. (j) completed UTA connector PCB 2. (k-i) PCB 2 interfaced with two PCB 1 transducer interfaces.

3.2 Multi-Transducer UTA Connection

In order to increase the number transducers that could be operated in parallel a multiplexing (MUX) system was added to support up to 6 transducers, shown in Figure 3-3. From Figure 3-3 it is clear how PCB 2 from the single transducer UTA connector interfaces with the MUX system. This allowed for parallel connection, but is limited to sequential use. Due to this board relying on the same fundamental UTA connection only 2 transducers can be activated at a time. The active transducer pair is controlled via a serial port.

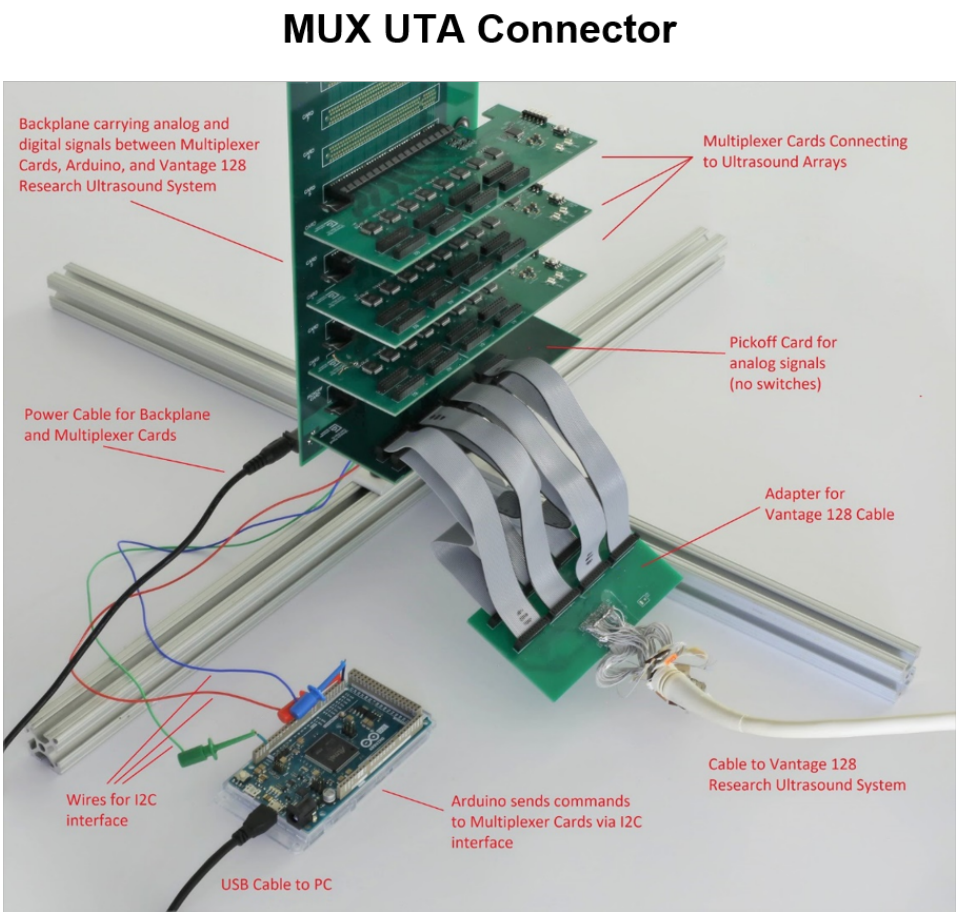

Figure 3-3: Labeled image of the multiplexing system

3.3 Experimental Setup

Ultrasound Flat Phantom

A flat ultrasound phantom model (Ultrasound Phantom Model 040GSE CIRS) was used to characterize the imaging performance of the transducers. As seen in Figure 3-4 this phantom consists of near field targets, resolution targets, hyperechoic and hypoechoic targets, along with various other targets. The main regions of interest imaged across all the transducers are the axial/lateral resolution targets and the vertical targets.

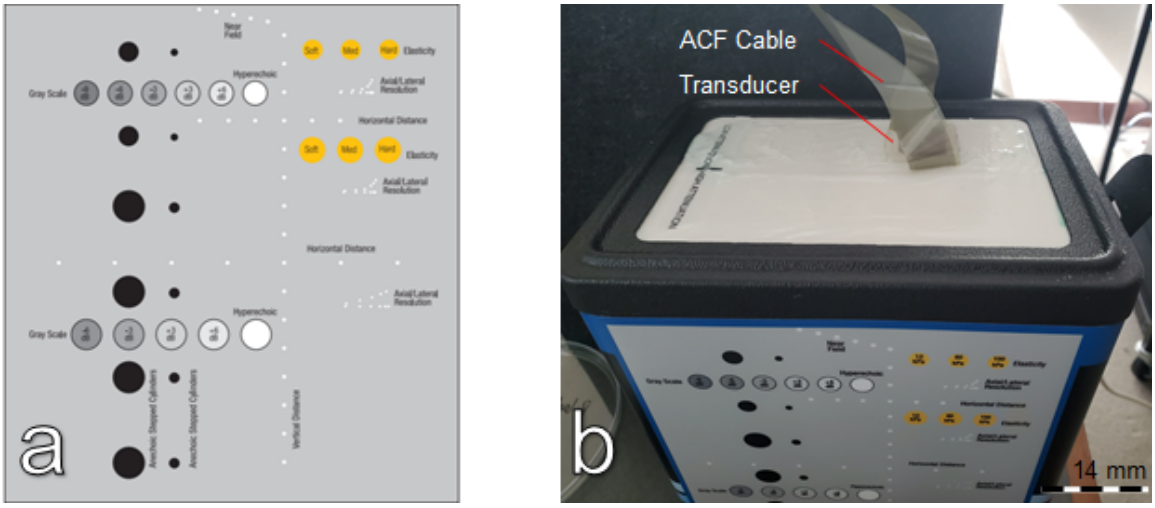

Figure 3-4: (a) Diagram of targets within CIRS phantom, (b) picture of phantom with single transducer

Methods

Each transducer was connected to the Verasonics system using the custom UTA connector and was driven with 50 V, and time-gain control activated. The excitation signal was a single cycle 3.5 MHz pulse. During the image acquisition a phased array beam forming scheme was used to obtain a real time image generated by the Verasonics system in order to visually align the transducer over the desired region on the phantom. After alignment was completed a SAR transmit/receive scheme was used and the raw received data was stored and beamformed in post-processing.

Finally, multiple arrays were placed and aligned on the phantom at measured intervals in order to obtain congregate images of the entire phantom. This was done by using the multi-transducer system and sequentially imaging with each transducer. Lastly, ultrasound gel was used during all the image acquisitions to ensure acoustic coupling between the transducers and phantom.

3.4 Results

A single transducer is capable of scanning a region of 15 cm deep and 12 cm wide as seen in Figure 3-5. However, the brightness and resolution is not constant throughout

the image which is to be expected. The bright region in the top-center of each image correspond to the location of the physical transducer. Due to the ultrasound reflections that occur at the transducer-phantom interface there is a concentration of energy in the image. It is also worth noting that although none of the transducer have 100% yield on their electrical connection they are all able to form an image as seen in Figure 3-6.

While each transducer successfully forms an image, the image quality among the different transducers varies. Transducer 2 and 4 appear to have the best resolution and contrast, while transducer 7 appears to have a strong spreading artifact. Nevertheless, the resulting images in Figure 3-7 from operating three arrays in series arises to excellent results. The over all field of views is increased without the need for any additional motion as in Figure 3-5.

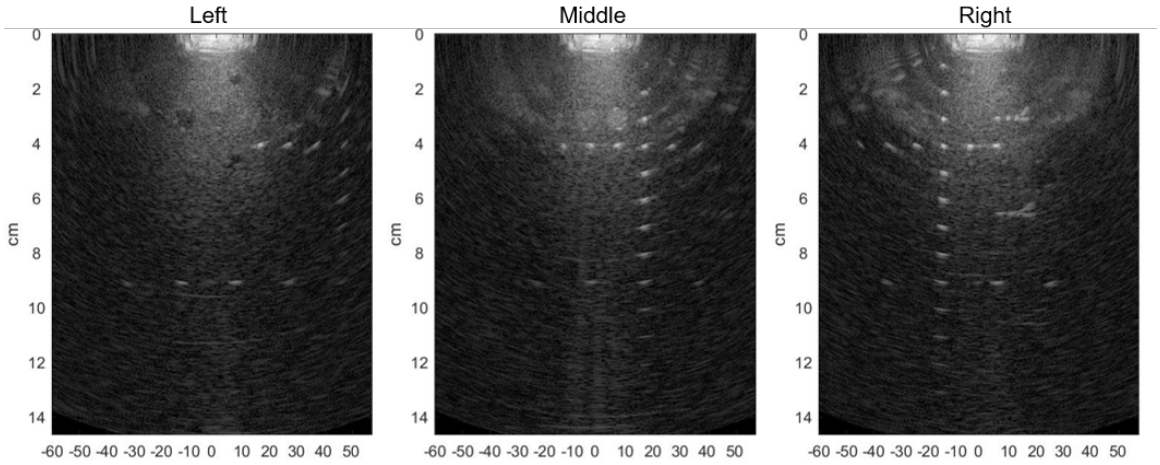

Figure 3-5: Scan of CIRS phantom at three locations with a single transducer using an 80db range

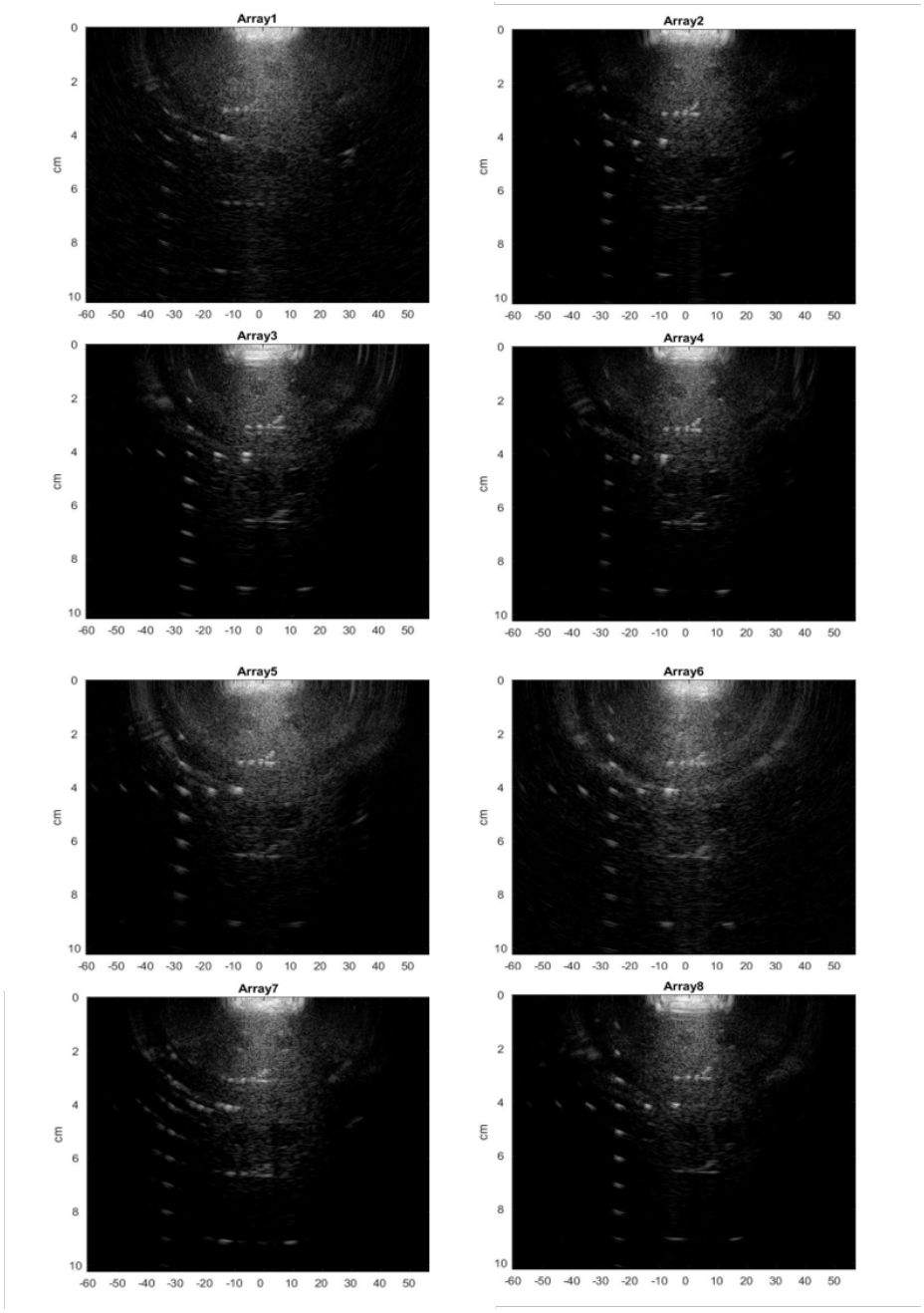

Figure 3-6: Summary of resolution target imaging of 8 transducers all with a 60 dB range

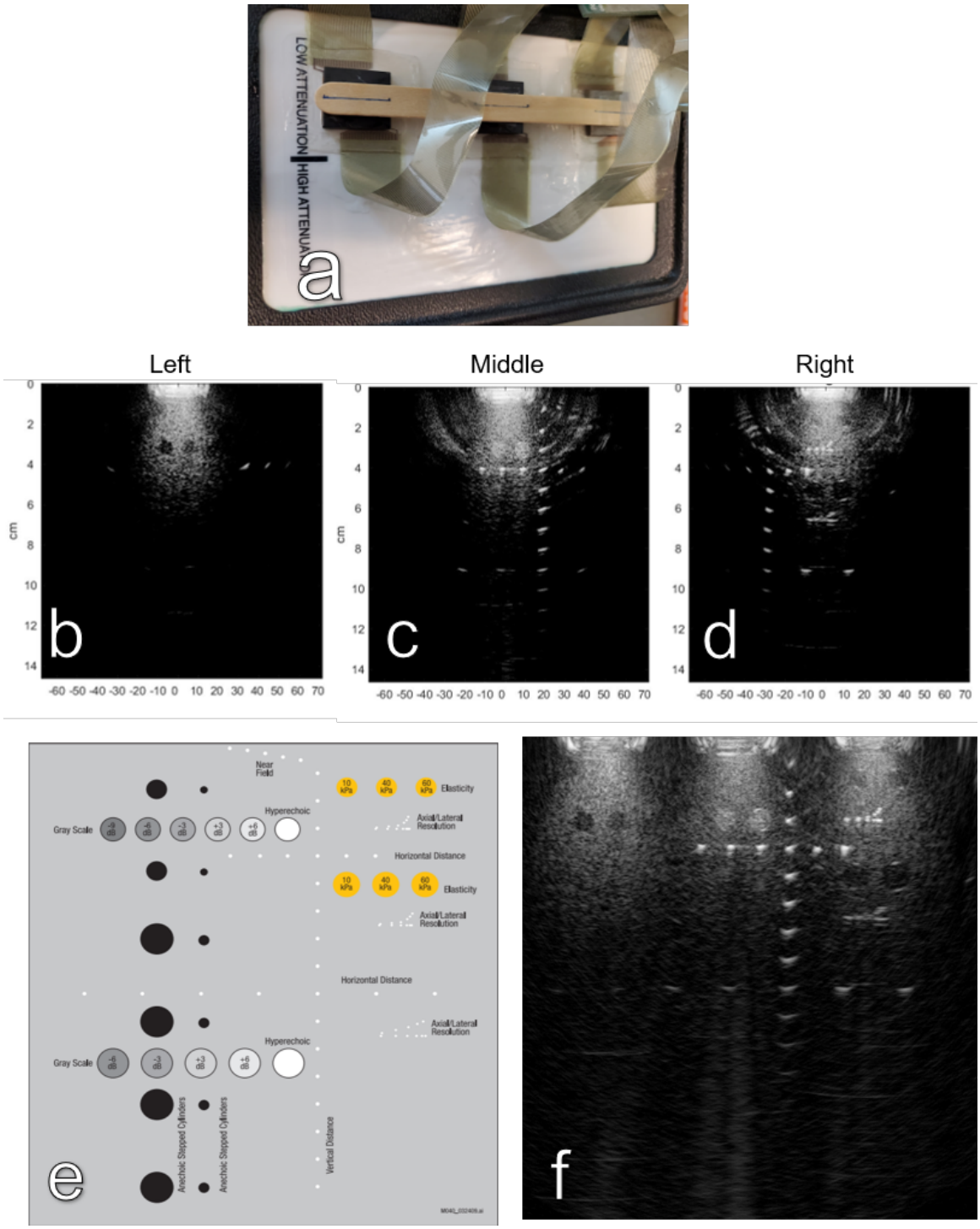

Figure 3-7: Scan of CIRS phantom at three locations with three different transducers (a) picture of the transducers on the phantom (b-d) individual images(e) CIRS phantom diagram (f) combined images

Chapter 4

Ultrasound Imaging on Curved Surface

Given the promising results in image quality on the CIRS flat phantom, the next step is to integrate the individual transducers into a conformable substrate. This results in a final system that is locally rigid, but globally flexible. While there are many applications that could benefit from conformable devices that allow for operator independence, each would require a custom design. Therefore, in this study a method for integrating the transducers into a conformable substrate was developed, as well as a 3D visualizer to aid in determining optimal design. This chapter will describe how these methods and tools were used to design a 5-transducer conformable patch for imaging on a curved phantom with three dimensional complex targets, as well as discuss the resulting acquired images and performance.

4.1 Conformable Patch

Curved Phantom

A curved phantom (US-18 Fundamental Ultrasound Phantom, Kyoto Kagaku) is the target for this study. It consist of various 3D object scattered through the material as seen in Figure 4-1. The surface of this phantom can be described as an ellipsoid

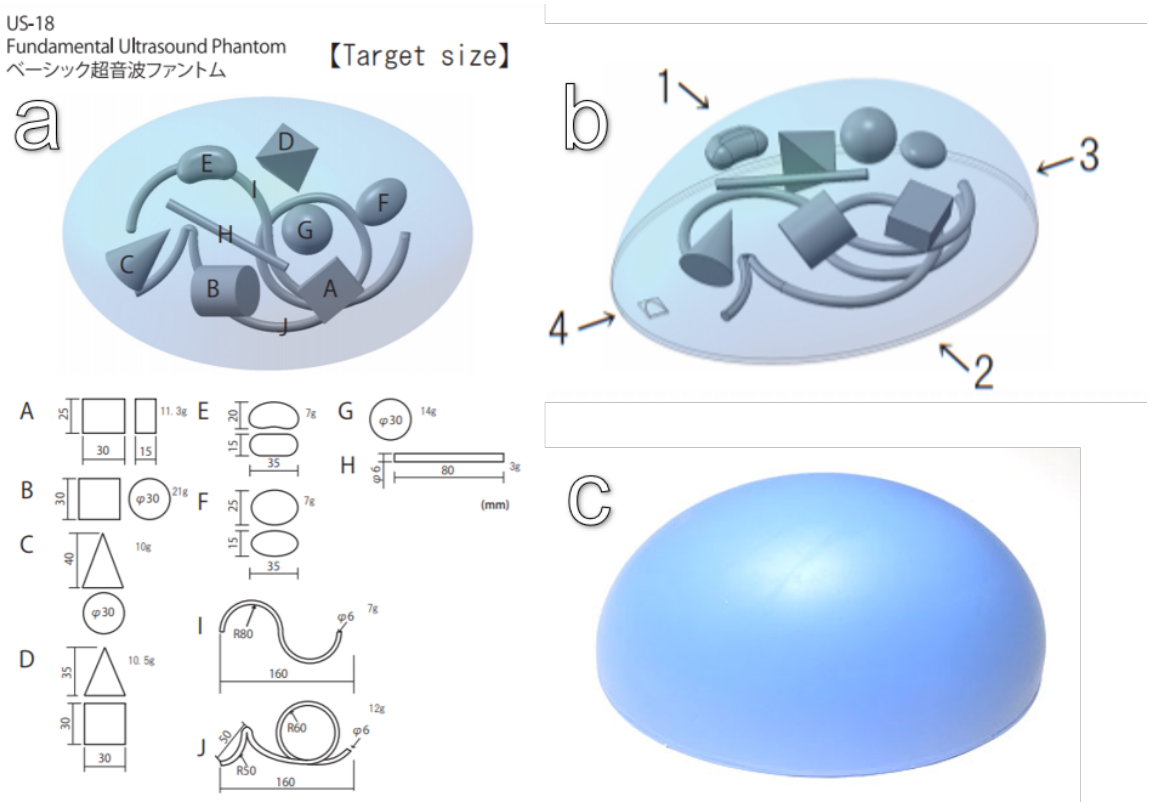

Figure 4-1: (a) Picture of curved phantom, (b) description of targets within phantom, (c) image of the phantom

as seen in equation 4.2 where the parameters are defined as follows in units of mm:

$$X_C = 0; Y_C = 0; Z_C = 0; X_R = 120; Y_R = 80; Z_R = 110 \tag{4.1}$$

$$\frac{(x - X_C)^2}{X_R^2} + \frac{(y - Y_C)^2}{Y_R^2} + \frac{(z - Z_C)^2}{Z_R^2} = 1 \tag{4.2}$$

The exact dimensions of the embedded targets are described in Figure 4-1, however their exact locations within the phantom are not provided. Given the lack of information on exact location of targets within the phantom, the C5-2 commercial probe was used to scan the phantom and identify targets of interest.

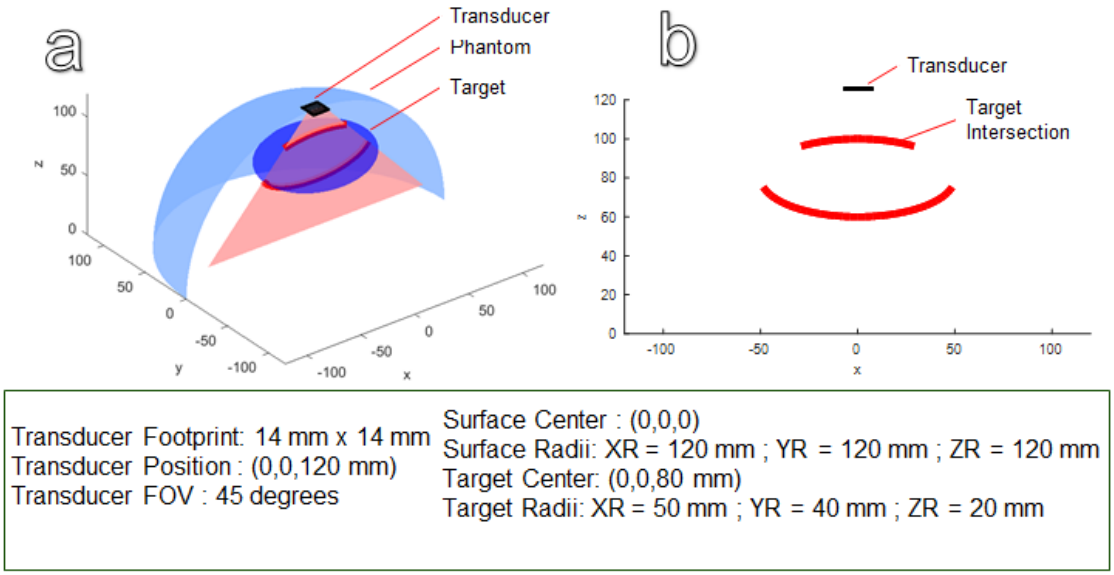

Figure 4-2: (a) 3D visualization of a single transducer over a spherical surface with an ellipsoid target (b) Intersection between transducer beam and target

Visualization

Visualization is a great way to gain insight into how the geometric properties of both the conformable patch and the surface interact. This visualization tool uses Matlab to render a 3D model of the FOV of one or more transducers within a phantom. Figure X(a) is a 3D render of a single transducer at the center of a spherical phantom with an ellipsoid as the target while Figure X(b) shows the 2D intersection between the transducer's FOV and the target. The intersection estimates the resulting perspective of the transducer's ultrasound image. All calculations and 3D rendering is performed in Matlab.

There are three main components to the visualizer: 1. an outer surface 2. the transducer set and respective beams 3. an embedded 3D target. The outer surface is defined as a surface in this case an ellipsoid as in 4.2 specified by its center and radii in the x, y, and z direction. A transducer is defined by a footprint, a location, and FOV. The location is constrained to a position on the defined outer surface, and the FOV is defined by an angle calculated as seen in Figure 4-3. The embedded 3D target is defined in the same way as the outer surface with differing parameters.

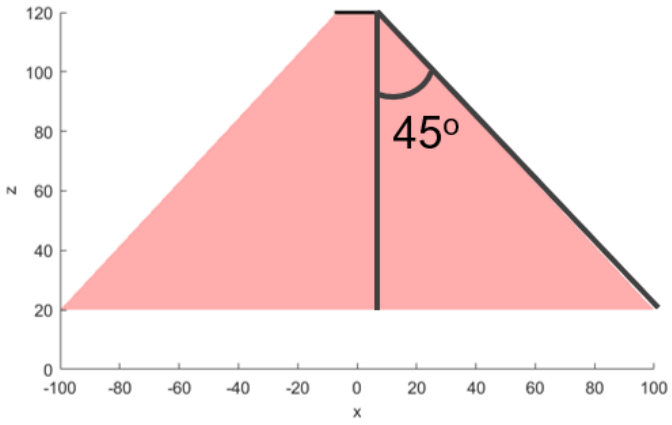

Figure 4-3: Definition of a transducer's FOV in the visualizer

Design

The identified functional requirements for a conformable patch were as follows:

(1) Conform to curvilinear surfaces

(2) Provide interface that allows ultrasonic transmission

(3) Bounded spacing between transducers

(4) Biocompatiblity

(5) Provide wide field of view

The proposed design is described in Figure 4-4(a) and consists of five transducers organized in a cross shape. The horizontal row of transducers are all oriented in the

Figure 4-4: 3D rendering of patch mold

same direction while the column of transducers are rotated 90 degrees. This results in an aggregate increase in field of view in both the X and Y axis. Additionally the petal-like designs allows for each transducer region to conform along its axis while minimizing global deformations.

In order to fabricate this a mold was designed and 3D printed. As seen in Figure 4-4(b), this mold consists of 5 elevated platform measuring 28mm X 28mm X 4.5mm and a smaller platform above it measuring 20mm X 20MM X 0.5mm. This allows for a thin layer to form that will serve as a window for the transducer to transmit ultrasonic waves that is less than 0.5mm thick. This thin layer additionally provides acoustic coupling between the transducer and the target surface, which minimizes the need for ultrasound gel. The patch itself is made out of a two-component silicone rubber (EcoFlex 03-00, Smooth-On) which cures at room temperature and is certified skin safe.

Fabrication

First, the mold was sanded to prevent all of the texture from the 3D printing process to create an imprint on the patch. Then, 50ml of the silicone rubber (EcoFlex 03-00) is mixed and poured into the mold which is enough to fill the mold without overflowing.

Figure 4-5: Mold fixed onto the shaker

The elevated platforms not only serve as the cavity, but also defines the thickness of rubber covering the transducer. The target thickness is 0.5mm, however, due to the viscosity and surface tension of the silicone rubber (EcoFlex 03-00 this cannot be achieved by directly pouring into one location on the mold.Instead, the rubber is partially poured over each of the 5 pillars and then the entire mold is placed on a shaker(VWR Advanced Vortex Mixer) for 10 minutes to provide an even covering of the pillars' surfaces as seen in Figure 4-5. Next the remaining rubber is poured into the mold and left to cure for 4 hours after which it is unmolded. Because the pot life of this silicone rubber is 45 minutes this process must be done quickly. The cured and unmolded silicone rubber patch is show in Figure 4-6.

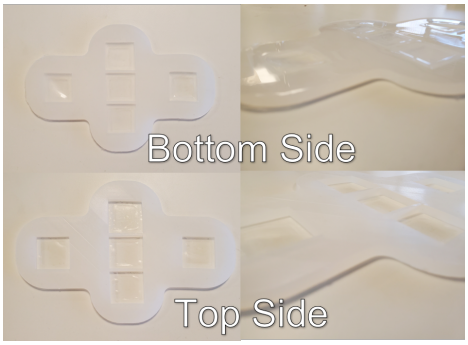

Figure 4-6: Silicone rubber conformable patch prior to the embedding of the transducers

The next step in the fabrication is to place and embed the transducers into the patch. After placing the device inside their respective cavities it is necessary to press out any air bubbles that might be trapped between the silicone and the matching layer. If any air bubbles remain it will diminish the overall acoustic energy being delivered as well as cause bright artifacts in the acquired images.

4.2 Imaging Methods

In order to obtain images, the MUX UTA connector was used to interface with all five transducers on the conformable patch. The patch was a aligned with curved phantom and carefully placed ensuring to minimize bubble accumulation at the interface (see

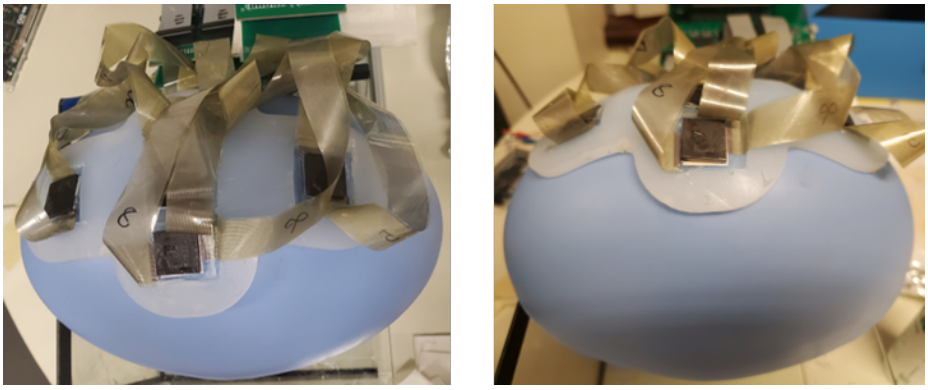

Figure 4-7: Conformable 5 transducer patch placed over the center of the phantom

Figure 4-7. Data was acquired from each transducer independently using the same parameters: A single cycle, 50V, 3.5MHz pulse. Next, the commercial C5-2 probe was used to obtain images over the same area to use as a comparison. Multiple levels of pressure were used on the commercial probe as seen in Figure 4-8(b)

Given the complex distribution of 3D target, the next set of images consisted of using a single transducer to scan the phantom. After identifying a region of interest three transducers were aligned and used to image. To facilitate the motion ultrasound gel was added at the transducer-phantom interface, however once multiple transducer were aligned the gel was removed and a thin layer of silicone rubber was used as the coupling medium as when in the patch.

4.3 Results

The commercial transducer was used to scan the entire phantom and identify target locations. Images over the spherical targets are shown in Figure 4-8. Additionally, Figure 4-8 also gives insight into how much pressure is required to obtain an image with the commercial. Despite this transducer having 128 elements, when no pressure is applied its convex shape limits its contact area. This reveals another limitation of commercial probes, that is addressed in the proposed system.

In Figure 4-7 a photo of the conformable patch with the 5 transducers inside the cavities are shown. This setup did not result in successful acquisitions of images

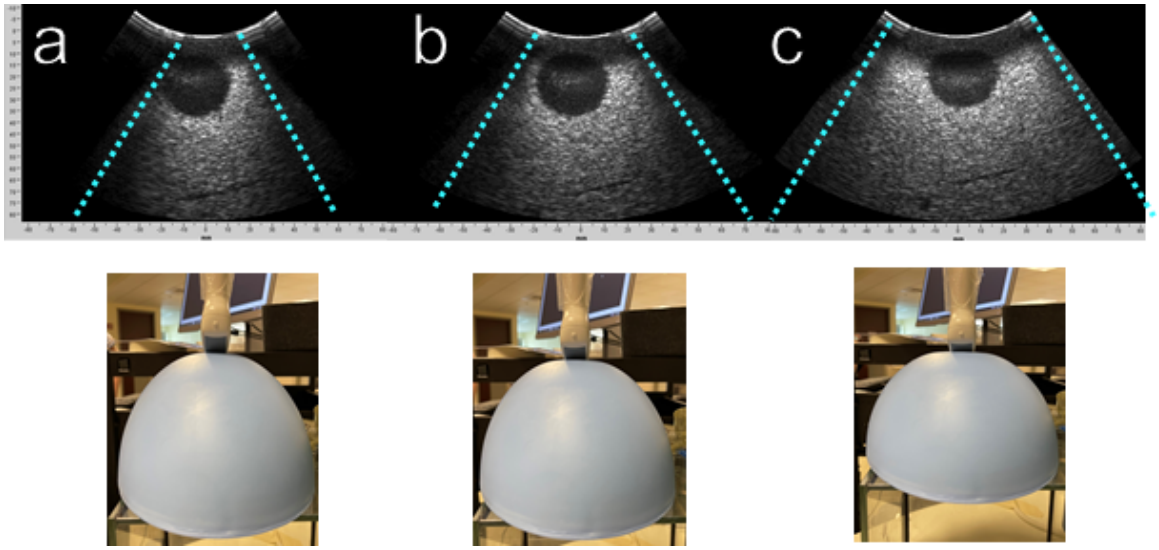

Figure 4-8: Resulting images with commercial probe while varying degrees of pressure are applied

due to the transducer not being fully embedded in the silicone rubber. This caused detachment from the thin layer of silicone between the transducer and the phantom resulting. Due to the decoupling between the transducer and the phantom all images acquired were mostly made up of noise.

During the single transducer translation understanding of the 3-D targets was understood by obtaining images after each small translation. In Figure 4-9(a-d) the transducer is being translated and different cross section of the sphere are evident.

Finally, a linear region on the surface was identified that interfaced with two 3-D targets: the sphere and ellipsoid. In Figure 4-10 an estimated model of this

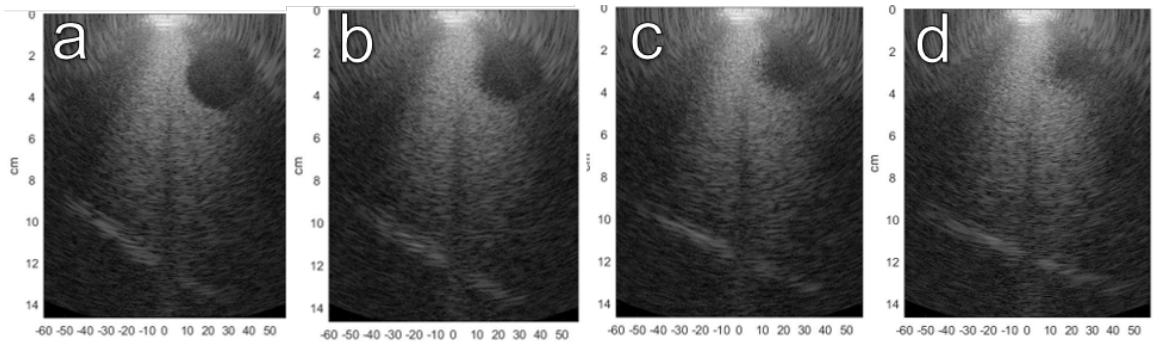

Figure 4-9: Ultrasound image set of a 3-D spherical target as it moves out of the FOV as the transducer moves

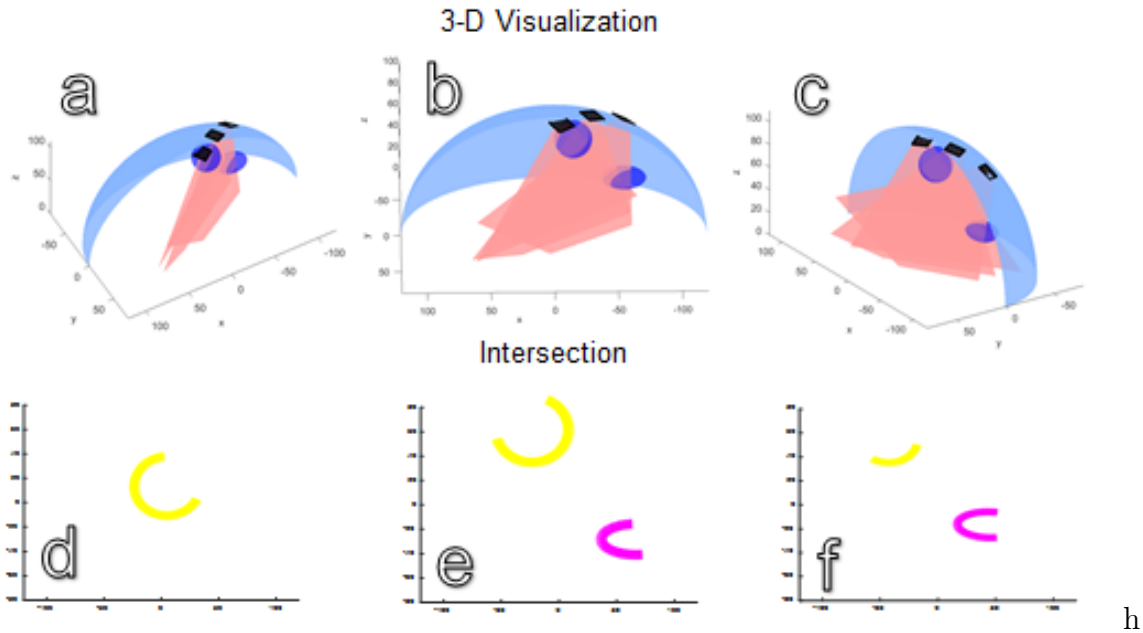

h

Figure 4-10: (a-c)Visualization of the 5-transducer patch over an estimate of the curved phantom (d-f) intersection between each transducer and the sphere (yellow) and/or ellipsoid (purple)

scenario is visualized from this it is clear that depending on the specific locations of the transducers how much of either object the transducer could see. However, by properly aligning three transducer a broader field of view can be obtained that observes both targets as seen in Figure 4-10(d-f) and Figure 4-11.

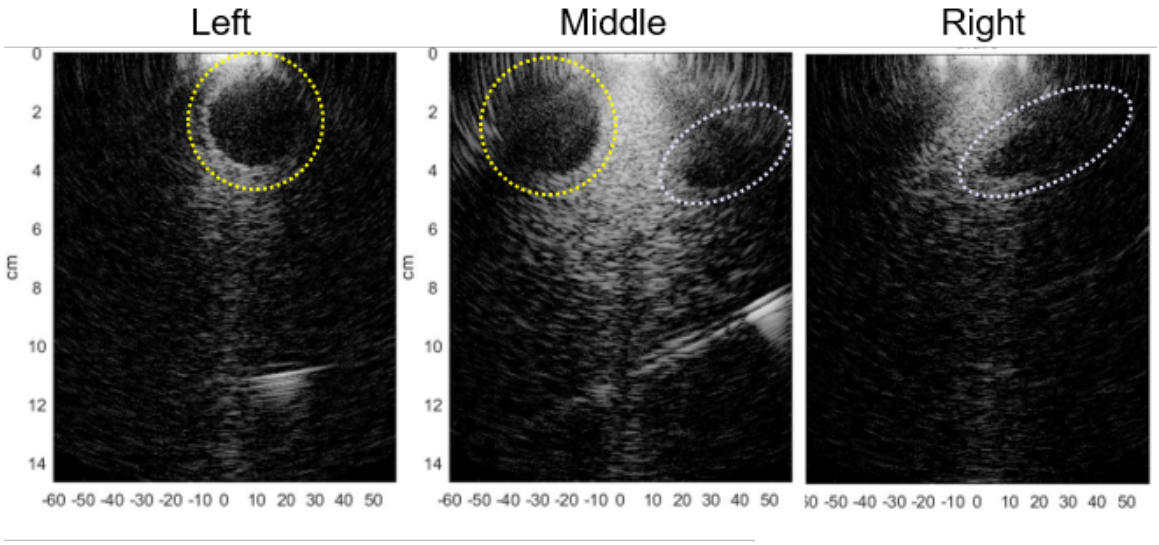

Figure 4-11: Image set taken by three aligned transducers overlapping the spherical (yellow dashed circle) and elliptical targets (purple dashed circle)

Chapter 5

Conclusion

Eight ultrasound transducers made up of novel piezoelectric ceramics were fabricated and characterized. The characterization consisted of electrical impedance, acoustic performance, pulse/echo waveform, and imaging of resolution targets. Additionally, a method for combining arrays into a conformable patch made out of silicone rubber was described and tested. Additionally, the performance of imaging over a curved surfaced was also tested.

The transducer characterization revealed a variation in performance likely cause by fabrication inconsistencies and connection degradation. Further work on fine tuning the fabrication is need to minimize this fluctuation. One change that could be done in order to attain a more robust connection is moving away from ACF cables and instead using a flexible printed circuit board. Lastly, more work is needed to be done in integrating the connections into the flexible substrate to ensure a more robust system and minimize mechanical detachment.

Bibliography

[1] *Output Measurements for Medical Ultrasound*. Springer London, 1991.

[2] David B. Bennett, Martin O. Culjat, Brian P. Cox, Aaron E. Dann, Kimani Williams, Hua Lee, Elliott R. Brown, Warren S. Grundfest, and Rahul S. Singh. A conformal ultrasound transducer array featuring microfabricated polyimide joints. *Health Monitoring of Structural and Biological Systems 2009*, 7295(April 2009):72951W, 2009.

[3] Hyun Joong Chung, Matthew S. Sulkin, Jong Seon Kim, Camille Goudeseune, Hsin Yun Chao, Joseph W. Song, Sang Yoon Yang, Yung Yu Hsu, Roozbeh Ghaffari, Igor R. Efimov, and John A. Rogers. Stretchable, multiplexed pH sensors with demonstrations on rabbit and human hearts undergoing ischemia. *Advanced Healthcare Materials*, 3(1):59–68, 2014.

[4] Bryan W. Cunitz, Barbrina Dunmire, and Michael R. Bailey. Characterizing the Acoustic Output of an Ultrasonic Propulsion Device for Urinary Stones. *IEEE Transactions on Ultrasonics, Ferroelectrics, and Frequency Control*, 64(12):1818–1827, 12 2017.

[5] Canan Dagdeviren, Pauline Joe, Ozlem L Tuzman, Kwi-Il Park, Keon Jae Lee, Yan Shi, Yonggang Huang, and John A Rogers. Recent progress in flexible and stretchable piezoelectric devices for mechanical energy harvesting, sensing and actuation. *Extreme Mechanics Letters*, 9:269–281, 2016.

[6] Canan Dagdeviren, Yan Shi, Pauline Joe, Roozbeh Ghaffari, Guive Balooch, Karan Usgaonkar, Onur Gur, Phat L. Tran, Jessi R. Crosby, Marcin Meyer, Yewang Su, R. Chad Webb, Andrew S. Tedesco, Marvin J. Slepian, Yonggang Huang, and John A. Rogers. Conformal piezoelectric systems for clinical and experimental characterization of soft tissue biomechanics. *Nature Materials*, 14(7):728–736, 7 2015.

[7] Canan Dagdeviren, Yewang Su, Pauline Joe, Raissa Yona, Yuhao Liu, Yun Soung Kim, Yongan Huang, Anoop R. Damadoran, Jing Xia, Lane W. Martin, Yonggang Huang, and John A. Rogers. Conformable amplified lead zirconate titanate sensors with enhanced piezoelectric response for cutaneous pressure monitoring. *Nature Communications*, 5(1):1–10, 8 2014.

[8] Aaron E. Dann, David B. Bennett, Rahul S. Singh, Jean-Jacques Lemaire, Warren S. Grundfest, and Martin O. Culjat. Fabrication of a conformal ring-annular ultrasound array. *Medical Imaging 2010: Ultrasonic Imaging, Tomography, and Therapy*, 7629(March 2010):76290R, 2010.

[9] M. T. Ghoneim, A. Nguyen, N. Dereje, J. Huang, G. C. Moore, P. J. Murzynowski, and C. Dagdeviren. Recent Progress in Electrochemical pH-Sensing Materials and Configurations for Biomedical Applications, 4 2019.

[10] John C. Gore. Foreword, 1 2014.

[11] Sahngki Hong, Yue Gu, Joon Kyo Seo, Joseph Wang, Ping Liu, Y. Shirley Meng, Sheng Xu, and Renkun Chen. Wearable thermoelectrics for personalized thermoregulation. *Science Advances*, 5(5), 5 2019.

[12] Xian Huang, Yuhao Liu, Huanyu Cheng, Woo Jung Shin, Jonathan A. Fan, Zhuangjian Liu, Ching Jui Lu, Gil Woo Kong, Kaile Chen, Dwipayan Patnaik, Sang Heon Lee, Sami Hage-Ali, Yonggang Huang, and John A. Rogers. Materials and designs for wireless epidermal sensors of hydration and strain. *Advanced Functional Materials*, 24(25):3846–3854, 7 2014.

[13] Dong Ik Kim. Preface: How dangerous are X-ray studies that we undertake every day?, 2016.

[14] Andrzej Nowicki. Safety of ultrasonic examinations; thermal and mechanical indices. *Medical Ultrasonography*, 22(2):203–210, 2020.

[15] Vida Pashaei, Alex Roman, and Soumyajit Mandal. Conformal Ultrasound Transducer Array for Image-Guided Neural Therapy. *2018 IEEE Biomedical Circuits and Systems Conference, BioCAS 2018 - Proceedings*, pages 1–4, 2018.

[16] Luana Persano, Canan Dagdeviren, Yewang Su, Yihui Zhang, Salvatore Girardo, Dario Pisignano, Yonggang Huang, and John A. Rogers. High performance piezoelectric devices based on aligned arrays of nanofibers of poly(vinylidenefluoride-co-trifluoroethylene). *Nature Communications*, 4(1):1–10, 3 2013.

[17] Stephen P Power, Fiachra Moloney, Maria Twomey, Karl James, Owen J O'Connor, and Michael M Maher. Computed tomography and patient risk: Facts, perceptions and uncertainties. *World Journal of Radiology*, 8(12):902, 2016.

[18] Rahul S. Singh, Martin O. Culjat, Stephen P. Vampola, Kimani Williams, Zachary D. Taylor, Hua Lee, Warren S. Grundfest, and Elliott R. Brown. Simulation, fabrication, and characterization of a novel flexible, conformal ultrasound transducer array. *Proceedings - IEEE Ultrasonics Symposium*, pages 1824–1827, 2007.

[19] Joshua Ray Windmiller and Joseph Wang. Wearable Electrochemical Sensors and Biosensors: A Review, 1 2013.

[20] Qi Zhang, Teng Ma, Congzhi Wang, Xiangli Liu, Yongchuan Li, Yu Chang, Jiamei Liu, Jiqing Huang, Yang Xiao, Tingrui Pan, and Hairong Zheng. Transformable Ultrasonic Array Transducer for Multi-scale Imaging and Beamforming. *IEEE Transactions on Industrial Electronics*, 0046(c), 2021.

[21] Shujun Zhang and Fei Li. High performance ferroelectric relaxor-PbTiO 3 single crystals: Status and perspective, 2 2012.